Soils and Foundations 2013;53(1):11–22

The Japanese Geotechnical Society

Soils and Foundations

www.sciencedirect.com
journal homepage: www.elsevier.com/locate/sandf

Seismic stability of embankments subjected to pre-deformation due to foundation consolidation

Mitsu Okamura[a,*], Shuji Tamamura[b,1], Rikuto Yamamoto[c,1]

[a]*Graduate School of Science and Engineering, Ehime University, 3 Bunkyo-cho, Matsuyama-shi 790-8577, Japan*
[b]*Toda Corporation, Japan*
[c]*Marugame City, Japan*

Received 6 October 2011; received in revised form 17 June 2012; accepted 27 July 2012
Available online 4 February 2013

Abstract

It has been reported that the major cause of earthquake damage to embankments on level ground surfaces is liquefaction of foundation soil. A few case histories, however, suggest that river levees resting on non-liquefiable foundation soil have been severely damaged if the foundation soil is highly compressible, such as thick soft clay and peat deposits. A large number of such river levees were severely damaged by the 2011 off the Pacific coast of Tohoku earthquake. A detailed inspection of the dissected damaged levees revealed that the base of the levees subsided in a bowl shape due to foundation consolidation. The liquefaction of a saturated zone, formed at the embankment base, is considered the prime cause of the damage. The deformation of the levees, due to the foundation consolidation which may have resulted in a reduction in stress and the degradation of soil density, is surmised to have contributed as an underlying mechanism. In this study, a series of centrifuge tests is conducted to experimentally verify the effects of the thickness of the saturated zone in embankments and of the foundation consolidation on the seismic damage to embankments. It is found that the thickness of the saturated zone in embankments and the drainage boundary conditions of the zone have a significant effect on the deformation of the embankments during shaking. For an embankment on a soft clay deposit, horizontal tensile strain as high as 6% was observed at the zone above the embankment base and horizontal stress was approximately half that of the embankment on stiff foundation soil. Crest settlement and the deformation of the embankment during shaking were larger for the embankment subjected to deformation due to foundation consolidation.

Keywords: Embankment; Liquefaction; Centrifuge test; Settlement

1. Introduction

Liquefaction of foundation soil has caused severe damage to a number of earth embankments during past earthquakes. River levees, which in nature are constructed on soft soil deposits on flood planes with shallow groundwater tables, are known as the most susceptible structures to seismic damage due to foundation liquefaction. The occurrence of crest settlement larger than half of the embankment height is not unusual (Matsuo, 1999). On the other hand, levees resting on non-liquefiable soil are considered to have rarely experienced severe damage. Crest settlement due to the deformation of soft foundation clay was, at the largest, 15% of the levee height during past earthquakes (River Front Center, 1999).

In 1993, the Kushiro-oki earthquake hit the northern part of Japan and the Kushiro River levee system was severely damaged. The incident attracted the attention of

*Corresponding author.
E-mail addresses: okamura@cee.ehime-u.ac.jp (M. Okamura), shuuji.tamamura@toda.co.jp (S. Tamamura).
[1]Former graduate student of Ehime University.
Peer review under responsibility of The Japanese Geotechnical Society.

Production and hosting by Elsevier

0038-0806
http://dx.doi.org/10.1016/j.sandf.2012.07.015

engineers since some parts of the damaged levee were underlain by a non-liquefiable peat deposit. It was presumed that the surface of the highly compressible and less permeable peat deposit below the levee had subsided in a concave shape, creating a saturated zone in the levee, as shown in Fig. 1 (Sasaki et al., 1995). The saturated zone in the bottom center of the levee might be highly susceptible to liquefaction due to the deformation that occurred prior to the earthquake. Considering a trapezoidal embankment, the vertical stress along the base line is the highest at the center. Thus, embankments inherently experience not only settlement, but also deformation in a concave shape due to uneven settlement of the foundation soil. This deformation mode results in reductions in horizontal stress and soil density at the lower part of the embankments. Since the liquefaction resistance of soil is approximately proportional to the mean effective stress (Ishihara et al., 1977), the reduction in horizontal stress may make embankment soil more liquefaction-prone. The reduction in the stress and the soil density of the embankments, as well as the increase in the thickness of the saturated zone of the embankments, all due to the subsidence of the foundation soil, are surmised as underlying mechanisms of the damaged levee.

More recently, over 2000 river levees were damaged by the 2011 off the Pacific coast of Tohoku earthquake (River Bureau, Ministry of Land, Infrastructure and Transport, 2011). A considerable number of levees failed in this mechanism. One such damaged levee is the left bank levee of the Naruse River located 31 km from the river mouth, which was approximately 9 m high and rested on a thick alluvium clay deposit. The crest settlement was larger than 5 m. A section of the damaged levee, illustrated in Fig. 2, was obtained through observations of the dissected cross section after the quake (Tohoku Regional Development Bureau, Ministry of Land, Infrastructure and Transport, 2011). The water table in the levee, observed 7 weeks after the earthquake with excavated boreholes, is also indicated in the figure. The material of the levee was mostly fine- to medium-loose sand with SPT N-values lower than 5. Several cracks and fissures appeared on the slope, which were partly filled with boiled sand, suggesting that the base of the levee had liquefied. It is interesting to note that an inspection of an adjacent undamaged levee, located about 100 m upstream of the damaged levee, revealed that the levee and the foundation soil conditions were very similar to those of the damaged levee in all aspects except for the water table in the levee being slightly lower (Tohoku Regional Development Bureau, Ministry of Land, Infrastructure and Transport, 2011). The loose saturated sand zone, with a thickness of about 1 m, liquefied and caused serious damage to the levee, but a slightly thinner zone did not liquefy. In current practice, the potential for liquefaction of a sand layer with a thickness of 1 m or less has often been ignored (e.g., Japan Road Association, 2001).

In this study, centrifuge tests are conducted to investigate the seismic stability of partly saturated embankments with and without the influence of deformation before shaking. The experimental data also provide a useful basis for calibrating a numerical analysis and for verifying design guidelines. Two aspects of the underlying mechanism are focused on in this study; one aspect is the thickness of the saturated zone. The possibility of the liquefaction of a thin saturated zone, with a thickness of only about 1 m, is experimentally investigated. The other aspect is the effect of the deformation and the associated change in stress of the embankments, due to foundation settlement, on the seismic stability of the embankments. The seismic responses of the embankments with and without imposed deformation, due to the consolidation of the foundation soil, are compared.

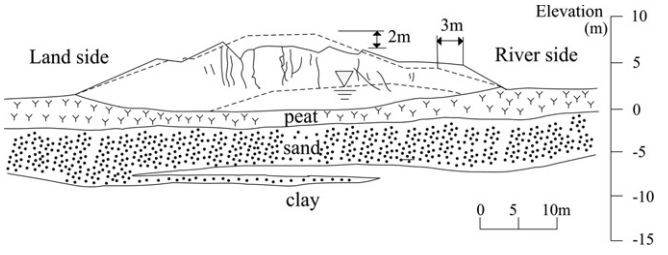

Fig. 1. Damaged levee of Kushiro River (after Sasaki et al., 1995).

2. Centrifuge tests

2.1. Model preparation and test conditions

In this study, the seismic responses of the models shown in Fig. 3 were tested in a centrifuge at 40g, where compacted uniform embankments, 80 mm high (3.2 m in prototype scale) and with 1:2 slopes, were resting on either

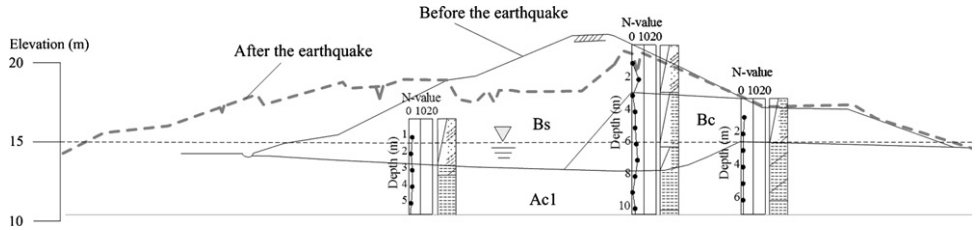

Fig. 2. Damaged levee of Naruse River (Tohoku Regional Development Bureau, Ministry of Land, Infrastructure and Transport, 2011).

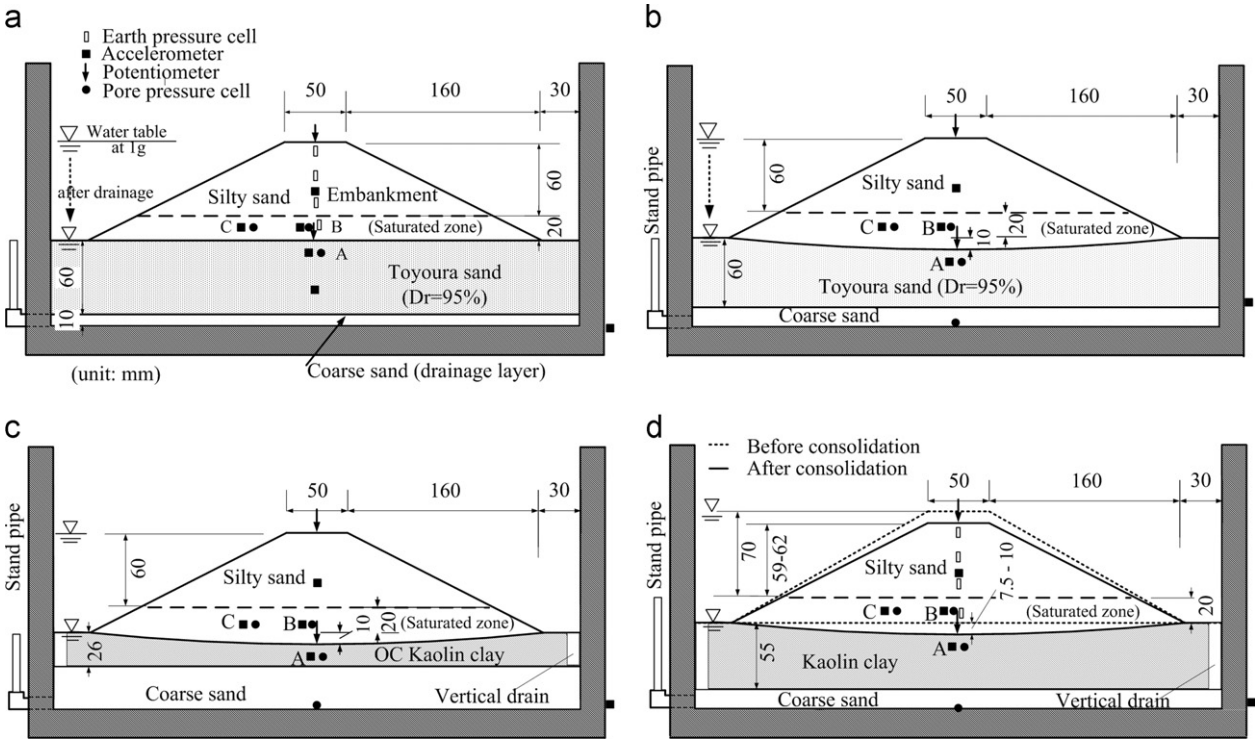

Fig. 3. Model configurations. (a) Model 1 (b) Model 2 (c) Model 3 (d) Model 4.

saturated dense sand or clay beds. The groundwater table was at the surface of the free field. A saturated zone of a certain thickness formed in the embankments due to the capillary rise (0.8 m in prototype) above the groundwater table, as will be described later. Model 1, indicated in Fig. 3(a), consisted of an embankment and an underlying dense sand layer. This model is the benchmark model experiencing neither settlement nor deformation of the embankment before base shaking was imparted. Model 4 is the uniform embankment compacted at the same density as Model 1, and resting on a soft clay deposit. The surface of the underlying clay was level at 1g before starting the centrifuge and subsided, as shown in Fig. 3(d), at the centrifuge environment of 40g. The dotted and solid lines in the figure illustrate the model shape at 1g and at 40g, respectively, just before shaking. The embankment of Model 4 was constructed to be 10 mm higher than that of Model 1, so that the shape and the dimensions of the two embankments, that is, height, slope angle and crest width, would be the same when the models were finally shaken after the consolidation process in the centrifuge.

A comparison of Models 1 and 4 provides insights into the combined effects of the deformation of embankments and the thickness of the saturated zone in embankments, that is, 0.8 m for Model 1 and 1.1–1.2 m for Model 4 in prototype scale. In order to investigate these effects individually, two more types of models were tested. In Model 2, shown in Fig. 3(b), the embankment was compacted at the same density as Model 1 and to the same shape and dimensions as those of Model 4 after consolidation. The embankment was set on dense sand with the surface finished up to a concave shape, also identical to the shape of the clay surface of Model 4 after consolidation. Model 3 was made to be the same as Model 2 in all aspects, except the soil type of the foundation. The foundation soil of Model 3 was made of kaolin clay with the surface finished up in a concave shape at 1g. The clay, with a smaller thickness, was overconsolidated so that the consolidation settlement in the centrifuge would be minimal. The embankments of Models 1, 2 and 3 had the same densities without experiencing deformation in the centrifuge before shaking, but different thicknesses of the saturated zone in their embankments. Also, the embankments of Models 2 and 3 had different drainage boundary conditions at the base of the embankments; the base of the saturated zone of the Model 2 embankment allowed pore fluid to migrate toward or from the foundation soil during shaking events, while the base of the Model 3 embankment had essentially an undrained boundary. A comparison of these 3 models reveals the effects of the thickness and the drainage boundary conditions of the saturated zones in the embankments.

The soil used to build the foundation layer of Models 1 and 2 was Toyoura sand. Dry sand was pluviated through air and compacted to a relative density of 95% in a rigid container with internal dimensions of 420 mm in width, 230 mm in depth and 120 mm in length. The surface of the layer was carefully leveled for Model 1, while it was finished in a concave shape for Model 2 using a vacuum. For Model 3, the de-aired slurry of kaolin clay, with a plasticity index of $Ip=27$, was consolidated to a vertical pressure of 100 kPa. For Model 4, the kaolin clay was consolidated to 30 kPa for Tests 4-1 and 4-2, and 20 kPa

for Test 4-3, as will be described later. The surface of the clay was leveled for Model 4, while it was finished in a concave shape for Model 3 before the embankments were set on it.

The soil used to construct the embankments was a non-plastic silty sand, of which the maximum dry density obtained from the proctor test was $\gamma_{d\text{-}max}=1.69$ g/cm^3. The grain size distributions of the sand are shown in Fig. 4. About 40% by weight of the particles of this silty sand were smaller than 0.06 mm, but the fines particles were composed predominantly of quartz with small amounts of feldspar, but no clay minerals. Special attention was paid to make the embankment quality the same throughout the test series. If the same compaction energy is provided in constructing embankments on foundation soils with different levels of stiffness, the density of the completed embankments may be different. In this study, the silty sand was prepared at a water content of 5% and compacted in a wooden mold of a trapezoidal shape to a dry density of 92% the maximum dry density. The base of the embankments for Models 1 and 4 was made flat, while the base of Models 2 and 3 was finished in a convex shape. The permeability of the embankment soil for the saturated condition was 3.1×10^{-6} m/s. The embankment in the mold was frozen in the refrigerator, set on the foundation layer in the container box and thawed at room temperature.

During the sample preparation, accelerometers (Type ASM-200 from Kyowa Electronic Instruments Co. LTD.) and pore pressure cells (Type P303AV-2 from SSK Co. LTD.) were installed at the proper locations and orientations. Potentiometers, to measure the settlement of the embankment crest and base, were also set. The settlement of the embankment base was measured as follows. During the construction of the embankment, a 2-mm-diameter plastic casing pipe was installed vertically passing through the embankment. A 15-mm-diameter thin plate was placed at the end of the casing pipe on the embankment base. After the embankment was set on the foundation soil, the potentiometer was set and the rod of the potentiometer was placed on the thin plate through the casing pipe. In addition, in the embankments of Models 1 and 4, earth pressure cells (Type PSS-1KAE from Kyowa Electronic Instruments Co. LTD.) were equipped to measure the horizontal stress.

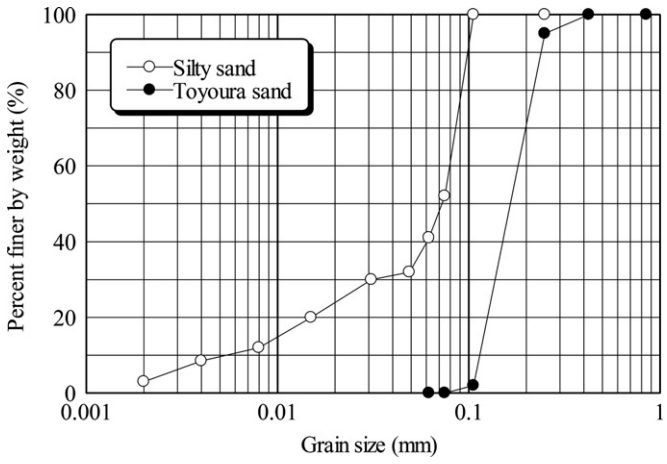

Fig. 4. Grain size distribution of soils used in model tests.

On completion of the thawing of the embankments, both the foundation soil and the embankments were fully saturated with a viscous fluid in the vacuum chamber, to a degree of saturation higher than 99.5%, which was measured with the method developed by Okamura and Kiyayama (2008) and Okamura and Inoue (2010). The viscous fluid was a mixture of water and hydroxypropyl methylcellulose (Type 65SH-50), termed Metolose by the Shin-etsu Chemical Company (Shin-etsu Chemical Co., Ltd, 1997). This Metolose solution pore fluid was prepared by dissolving 2% Metolose by weight in water, so as to achieve a viscosity of 50 times the viscosity of water (50 cst kinematic viscosity). The consequence of using the viscous fluid in the centrifuge tests at $40g$ to model the liquefaction of the water-saturated prototype embankment soil in the field was that the actual prototype permeability being simulated was $k_{prototype}=3.1\times10^{-6}/50\times40=2.5\times10^{-6}$ m/s (Tan and Scott, 1985). In the centrifuge modeling of a seismic event, it is normal practice to change the viscosity of the pore fluid to the same value as the level of g. In this study, however, a viscous fluid with 50 cst, instead of 40 cst, was employed. This is simply because data on the physical properties of the 50 cst Metolose solution had already been accumulated.

The model was set on the geotechnical centrifuge at Ehime University. The centrifugal acceleration was gradually increased to $40g$. The viscous fluid on the ground and in the pores of the embankment soil was drained through a stand pipe and the model was consolidated. In Models 3 and 4, a 20-mm-diameter sand drain was installed on both sides of the clay layer in order to accelerate the drainage rate of the excess fluid on the clay. On completion of consolidation and drainage of the excess pore fluid, the model was shaken horizontally with a mechanical shaker (Ishimaru et al., 2008). Three seismic events were imparted to each model with ample time intervals to dissipate the excess pore pressure generated in the preceding event. The acceleration time histories of the events have the basic shape indicated in Fig. 5, with peak accelerations of about $A_h=0.7$ or 1.0, 2.0 and 2.5 m/s^2, and lasted 20 s in the prototype scale. The shaking intensity was varied by changing the rotation rate of the cam shaft in the shaker. Thus, the predominant frequencies of the input motions were 0.75 Hz for $A_h=2.0$ m/s^2 and 1.0 Hz for $A_h=2.5$ m/s^2. The acceleration response spectra (5% damping) of several tests are indicated in Fig. 5(c). The input motion was repeated quite well from test to test. For instance, input motions with 0.75 Hz frequency and $A_h=2.0$ m/s^2 observed maximum input acceleration in all eight tests was in a small range between 2.05 m/s^2 and 2.22 m/s^2. A comparison of the input motions in the form of a time history is given in Fig. 5(d) for Tests 1-2 and 4-2. Although significantly different acceleration responses were observed in the soils of these models, the input motions were well reproduced.

The test conditions are summarized in Table 1. Four types of models, shown in Fig. 3, were tested in this study. With

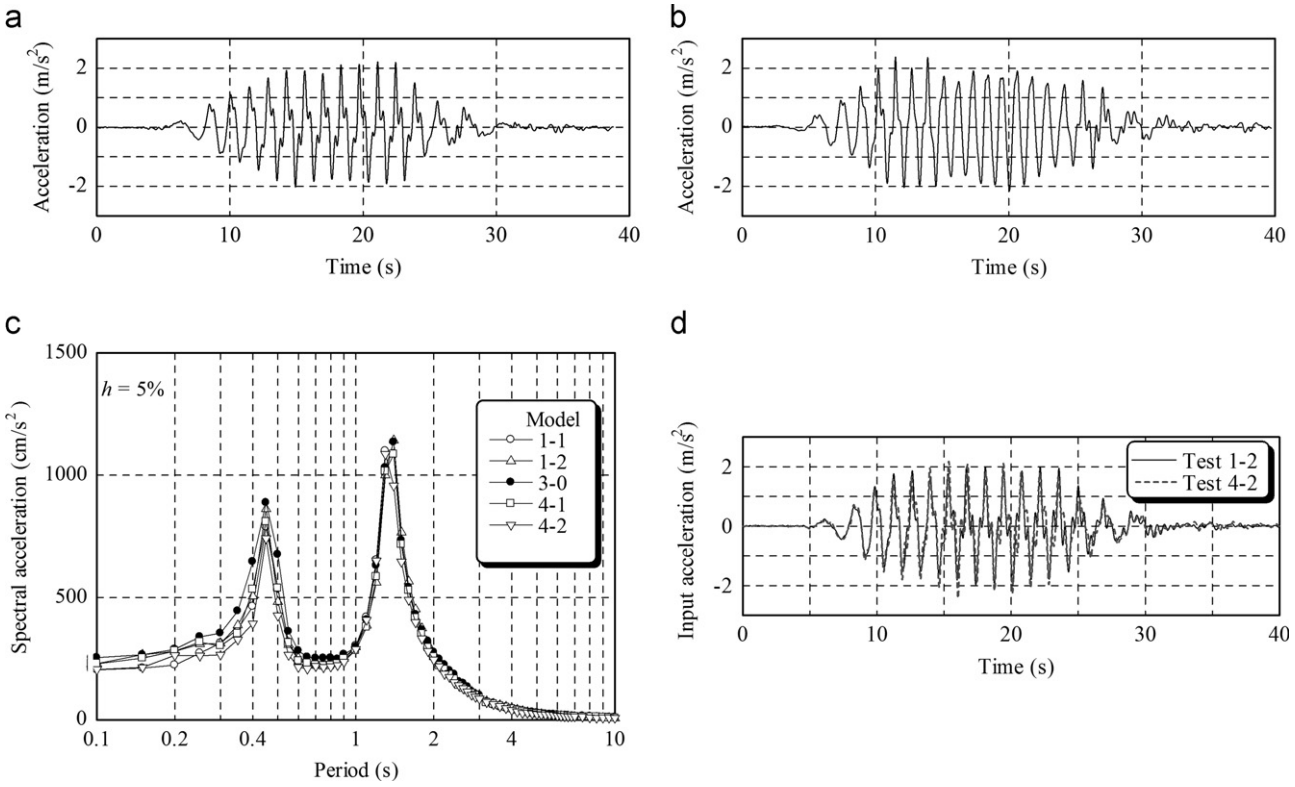

Fig. 5. Input acceleration time histories and response spectrum accelerations. (a) A_h=2.0 m/s^2 (b) A_h=2.5 m/s^2 (c) response spectrum accelerations (d) reproducibility of input acceleration (A_h=2.0 m/s^2).

Table 1
Summary of test conditions.

Model	Test code	Type of foundation soil	Pre-consolidation pressure (kPa)	Thickness of saturated zone in embankment (m)	Amplitude of input acceleration, A_h (m/s^2)
1	1-1	Dense sand		0.8	0.7, 2.0, 2,5
	1-2	Dense sand		0.8	1.0, 2.0
	1-3	Dense sand		0.8	0.7, 2.0, 2.5
2	2	Dense sand		1.2	0.7, 2.0,2.5
3	3	OC clay	100	1.2	0.7, 2.0,2.5
4	4-1	NC clay	30	1.1	0.7, 2.0, 2.5
	4-2	NC clay	30	1.2	1.0, 2.0
	4-3	NC clay	20	1.2	0.7, 2.0, 2.5

Represented in prototype scale.

regard to Models 1 and 4, the tests were repeated two or three times to confirm the reproducibility of the results. As for Model 4, Test 4-2 is a duplication of Test 4-1. For Test 4-3, the consolidation pressure at 1g was lower than that of Tests 4-1 and 4-2 so that the embankment would undergo larger settlement and deformation in the centrifuge before shaking.

2.2. Undrained cyclic strength and deformation characteristics of embankment soil

The liquefaction resistance of the silty sand was tested through a series of triaxial tests. All the tested specimens were prepared in the same way as the embankments and were fully saturated with water, with a Skempton's B value higher than 0.95, under an effective confining pressure of 98 kPa.

Fig. 6 depicts the relationship between the cyclic shear stress ratio, $\sigma_d/2\sigma'_c$, and the number of cycles to cause a double amplitude axial strain, DA, of 5%, where σ_d and σ'_c denote the axial stress amplitude and the initial effective confining stress, respectively. In this paper, the cyclic stress ratio to cause a 5% double amplitude axial strain in 20 cycles is termed as the liquefaction resistance. Although the soil was well compacted and in a dense state with the degree of compaction of 92%, the liquefaction resistance was relatively low.

2.3. Height of capillary rise in embankment

An additional centrifuge test was conducted to confirm the thickness of the saturated zone formed in the embankment due to the capillary rise. A model embankment, fully

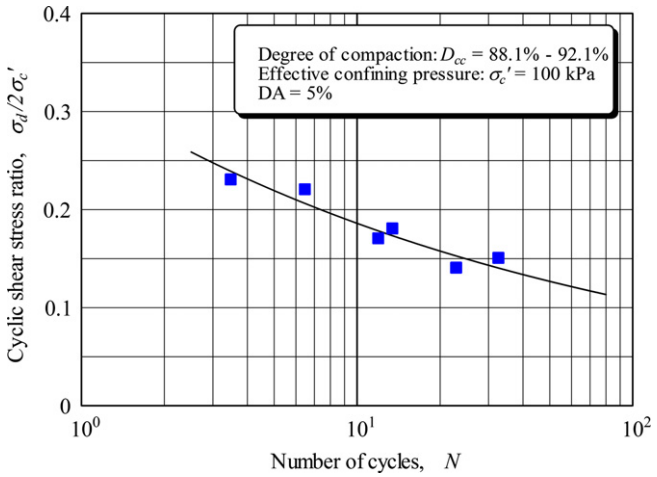

Fig. 6. Liquefaction strength and deformation characteristic of silty sand used for model embankment. (a) Liquefaction strength curve (b) deformation characteristic.

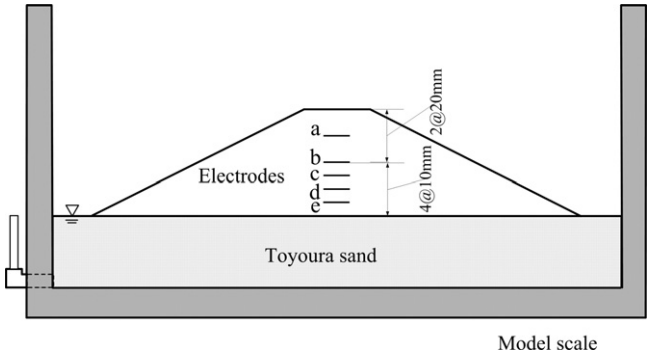

Fig. 7. Model configuration for dehydration tests.

saturated with the viscous fluid, was prepared as indicated in Fig. 7 in much the same way as Model 1. Five electrodes were set in the embankment. The centrifugal acceleration was increased step-by-step with ample time allowed in each step to dehydrate the pore fluid of the embankment while keeping the groundwater table at the surface of the free field. Fig. 8 shows variations in the apparent resistivity between adjacent electrodes. In the tests, a voltage of $V=5$ v was provided between a pair of adjacent electrodes, and the current, I, was measured. The apparent resistivity, V/I, started to increase and leveled off again as the centrifugal acceleration increased. Assuming that the void ratio of the embankment does not change, the change in the apparent resistivity directly correlates with the water content. It is interpreted that when the apparent resistivity started to increase at a certain centrifugal acceleration, the boundary between the saturated zone and the unsaturated zone was at the level of the upper electrode. Also, when the apparent resistivity leveled off, the boundary was at the level of the lower electrode. The height of the boundary or the capillary rise in the prototype sense, nH_m, was plotted against the centrifugal acceleration, n, in Fig. 9, where H_m denotes the height of the boundary from the surface of the free field in the model scale. The prototype height of 0.8 m

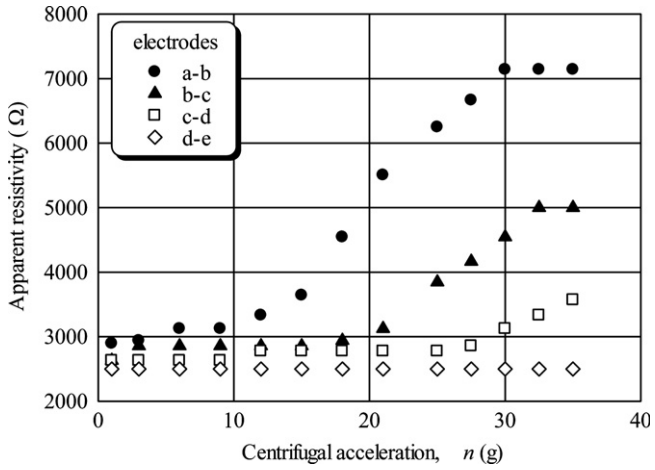

Fig. 8. Variations in apparent resistivity between adjacent electrodes.

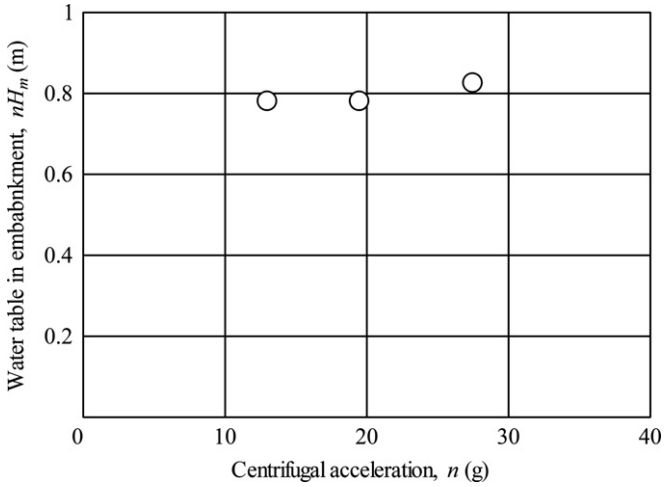

Fig. 9. Capillary rise in embankment at different centrifugal accelerations.

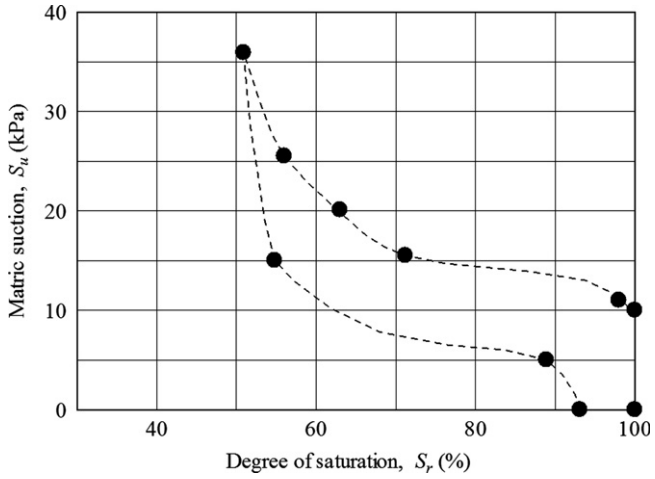

Fig. 10. Water retention characteristic curve of silty sand.

was constant irrespective of the centrifugal acceleration, confirming the validity of the similitude of the centrifuge testing regarding the capillary rise (Garnier, 2001). A water

retention characteristic curve, obtained from the pressure plate test on the silty sand, is shown in Fig. 10. It should be noted that the tested specimen was saturated with water instead of viscous fluid. The height of the capillary rise of 0.8 m in the embankment is somewhat lower than that assumed from the observed air entry pressure of 11 kPa in the pressure plate test. This discrepancy is believed to be due to the difference in surface tension between water and the viscous fluid. The surface tension of the Metolose solution used in the centrifuge tests was 5×10^{-3} N/m at a room temperature of 20 °C, which was roughly 70% that of water.

3. Results and discussions

All the tests on Models 1, 2, 3 and 4 were conducted at 40*g*. Hereafter, all the test results are represented in prototype scale unless otherwise mentioned.

3.1. Consolidation settlement and deformation before shaking

Fig. 11 indicates the recorded settlement at the crest and at the base of the embankments before the shaking events for Tests 1-1, 3 and 4-1. Note that the lines for the tests in this figure correspond to the different settlement scales along the ordinate axis. The settlement for all the tests is summarized in Table 2. The base settlement of the embankments on a dense sand bed (Models 1 and 2) was very limited in the range of 1 to 6 mm; this was also the case for the Model 3 embankment resting on stiff thin clay. The difference in settlement between the crest and the base, which corresponds to the deformation of the embankment, was in the range of 23 to 37 mm for Models 1, 2 and 3. The settlement of Models 1, 2 and 3 before shaking is considered small as compared to the height of the embankments, 3.2 m, and its effects on the thickness of the saturated zone and the stress distributions in the embankments are expected to be negligible, and thus, are not discussed in this paper. On the other hand, the base of the embankments of Model 4 (Tests 4-1, 4-2 and 4-3) subsided approximately 300–400 mm depending on the pre-consolidation pressure. Differences

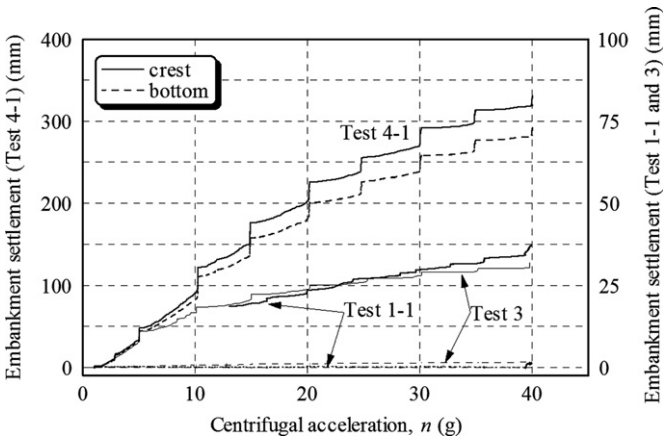

Fig. 11. Settlement at crest and base of embankment.

Table 2
Crest and base settlement until the base shaking imparted.

Test code	Settlement in prototype scale (mm)	
	Crest	Base
1-1	37	2
1-2	40	3
1-3	29	6
2	37	2
3	33	6
4-1	336	296
4-2	348	303
4-3	464	408

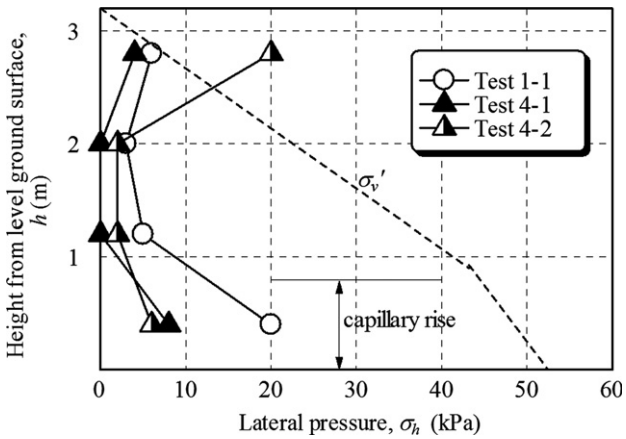

Fig. 12. Horizontal earth pressure at 40*g* on centerline of embankment.

in the settlement between the crest and the base were 40–45 mm for Tests 4-1 and 4-2, respectively, and 56 mm for Test 4-3. The deformation of the embankment was larger for the case with larger consolidation settlement.

The measured horizontal earth pressure, σ_h, along the centerline of the embankments at 40*g* just before shaking, are plotted against the height from the free field surface, h, in Fig. 12. The broken line in the figure corresponds to the profile of the vertical effective stress, σ'_v, estimated simply from the depth of the soil from the crest. As compared with Model 1, the reduction in horizontal stress in the Model 4 embankment was apparent at heights lower than 1.2 m. At $h=0.4$ m, considering the negative pore pressure of -4 kPa, the lateral effective stress, σ'_h, of the Model 4 embankment was about 11 kPa. The stress ratio is, $\sigma'_h/\sigma'_v=0.23$ and mobilized friction angle of 39° is close to the angle of shear resistance, $\phi'=41°$, obtained from drained triaxial tests on the saturated specimen prepared at the same density as the embankment.

Fig. 13 illustrates the sketch of the Test 4-3 embankment before and after consolidation, where the largest settlement during the consolidation process was observed in this study. Vertical and horizontal strain levels of the representative grids are given in Table 3. Horizontal tensile strain is observed at around the bottom center of the embankment (Grids (1) and (2)). The horizontal strain turns from negative at the base to

positive at the crest along the centerline. This strain profile is comparable to the above-mentioned stress distribution on the centerline. It should be noted that the volumetric strain of the soil in Grids (1) and (2) is negative, indicating that the soil at these locations loosened during foundation consolidation, while the soil densified near the crest.

3.2. Effects of thickness of saturated zone on seismic stability of embankment

In this section, the results of tests on Models 1, 2 and 3 are compared to discuss the effects of thickness and the drainage boundary condition of the saturated zone in the embankments. In these models, neither noticeable settlement nor excess pore pressure was generated by the shaking events of either $A_h=0.7$ m/s^2 or 1.0 m/s^2. Fig. 14 depicts the observed excess pore pressure at two locations in the embankments, labeled 'B' and 'C', as shown in Fig. 3, where the effective overburden pressures calculated from thickness of the soil just above the locations are $\sigma'_{v0}=46$ kPa and 35 kPa, respectively. Note that the excess pore pressure was -4 kPa before shaking because of the matric suction at the locations.

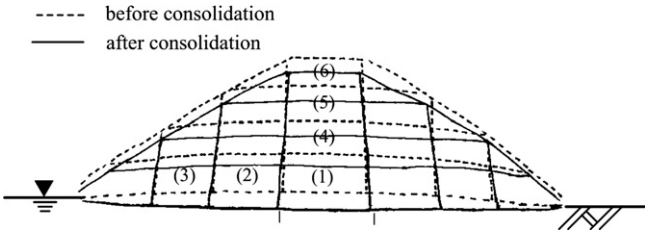

Fig. 13. Sketch of embankment of test 4-3.

Table 3
Strains in embankment due to foundation consolidation (Test 4-3).

Grid	Vertical strain (%)	Horizontal strain (%)
(1)	3	−6
(2)	1	−2
(3)	0	0
(4)	2	−3
(5)	0	−1
(6)	3	3

For the shaking event of $A_h=2.0$ m/s^2, the excess pore pressures for Tests 1-1 and 1-3 were considerably smaller than the effective overburden stresses, although a significant fluctuation is seen for Test 1-1. For Tests 2 and 3, in which the thickness of the saturated zone was 1.5 times larger than for Model 1, generated excess pore pressures were as high as the effective overburden stress at location 'C' suggesting that the sand liquefied. In these tests, similar pore pressure responses were observed at location 'B'. At location 'C', the excess pore pressure of Test 2 increased during the first half of the shaking event and leveled off at about $t=20$ s, while for Test 3 the excess pore pressure continued increasing throughout the shaking event. The different drainage conditions at the base of the saturated zone are responsible for the different pore pressure responses.

During the shaking event of $A_h=2.5$ m/s^2, the excess pore pressure levels were similar for Models 2 and 3. This may be due to the fact that the imparted shaking was strong enough to reach the ceiling of the excess pore pressure in both models. These results indicate that a

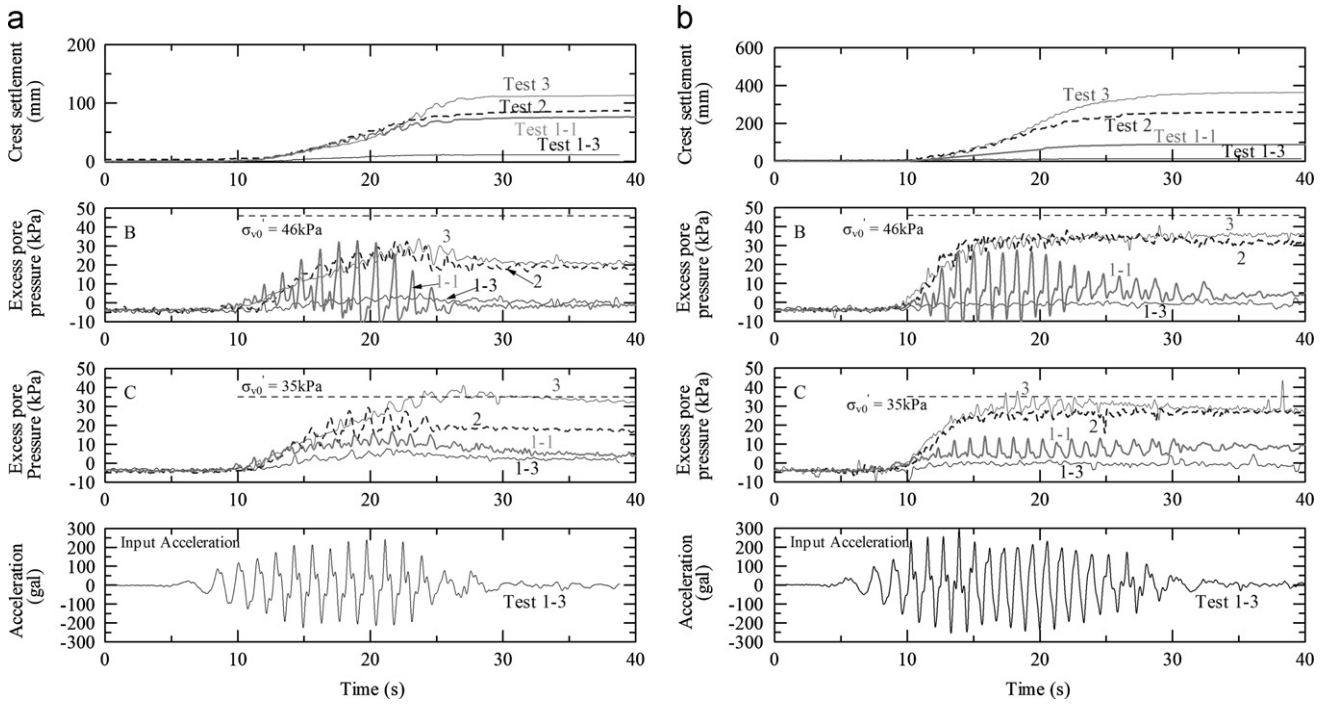

Fig. 14. Selected time histories of excess pore pressures and settlement of Models 1,2 and 3.

relatively thin saturated zone with a thickness of 1.2 m and with permeability of 2.5×10^{-6} m/s can liquefy during strong base shaking. The chance of liquefaction occurrence is sensitive to the thickness as well as to the drainage boundary conditions of the saturated zone.

It can also be observed in Fig. 14 that the crest settlement started to increase when the excess pore pressure reached about half the effective overburden pressure. The higher the generated excess pore pressure, the larger the rate of the crest settlement. The cumulative crest settlement is plotted against the maximum drainage distance of the saturated zone, D_d, in Fig. 15. For Models 3 and 4, in which the embankments were underlain by clay, D_d is the thickness of the saturated zone. For Models 1 and 2, D_d is half the thickness of the saturated zone, although excess pore pressure was generated to some extent in the underlying dense sand layer; and thus, the embankment base was not the perfect drainage boundary. The crest settlement was limited for the cases of D_d=0.4 m (Model 1) and sharply increased with the increase in D_d. It can be concluded that the thickness of the saturated zone has a significant effect on the crest settlement. For the particular sand material and test conditions employed in this study, D_d in the order of 0.4 m is the border below which liquefaction of the saturated zone and associated crest settlement does not occur. It should be mentioned that the total settlement of the embankment base due to shaking was 28 mm for Model 2 and less than 36 mm for Model 1. The crest settlement was mostly caused by the deformation of the embankments.

3.3. Effects of deformation due to foundation consolidation on seismic stability

The Model 4 embankments underwent a decrease in height and an increase in width during foundation consolidation. After the consolidation at 40g, the height of the embankment crest above the level ground surface for Model 4 was in the range of 3.2–3.3 m, which was approximately identical to those for the other models. The thickness of the saturated zone in the embankments was almost the same for Models 3 and 4, except for Test 4-1 in which the thickness was slightly smaller (see Table 1).

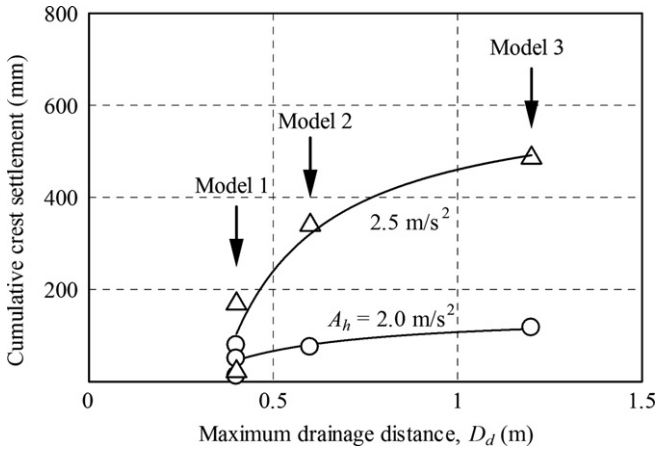

Fig. 15. Effects of thickness and drainage boundary condition on crest settlement.

The height and the shape of the surface of the foundation clay of Model 4, shown in Fig. 3(d), was obtained from careful observation of the exposed section of the model dissected after the test. Since the total settlement of the base of the embankment during the shaking events observed with the potentiometer was less than 29 mm, it is reasonable to assume that the height and the shape of the clay surface illustrated in Fig. 3(d) was not changed by the shaking.

Time histories of the observed excess pore pressure and the embankment settlement are shown in Fig. 16. In the first event, the imparted acceleration amplitude was about 0.7 m/s^2 and the generated excess pore pressure in the embankments as well as the crest settlement were not significant. In the second event, where the base shaking with the acceleration amplitude A_h=2.0 m/s^2 was imparted, the embankments fissured and deformed.

A few seconds after the shaking event of A_h=2.0 m/s^2 was initiated, the excess pore pressure of Model 4 was generated at a much higher rate than that of Model 3. The lower liquefaction resistance of the soil in the saturated zone of Model 4, due to the lower initial horizontal stress and the degraded soil density, is believed to be responsible for this. The excess pore pressure of Test 4-1 reached a plateau and leveled off shortly after the initiation of the shaking; however, the excess pore pressure of Model 3 continued to increase. The excess pore pressure in the latter half of the shaking was higher for Model 3 than for Model 4; however, the crest settlement was larger for Model 4. It has been reported that the excess pore pressure that can be generated in the foundation soil with an embankment is not always as high as the initial effective vertical stress (Uwabe et al., 1986; Koga and Matsuo, 1990; Okamura and Matsuo, 2002). Since the horizontal deformation of sand in the soil is not confined, the total horizontal stress is not able to reach the total initial vertical stress even during strong shaking. In other words, the generated excess pore pressure in the soil depends also on the horizontal stress. This is believed to also be the case for the soil in embankments. The lower initial horizontal stress in Model 4 is a possible reason for the lower excess pore pressure.

The cumulative crest settlement of all the tests conducted in this study is plotted against the input acceleration amplitude, A_h, in Fig. 17. The only difference in the test conditions between Models 3 and 4 is the consolidation settlement before shaking. Therefore, it is interesting to plot crest settlement against consolidation settlement, as shown in Fig. 18. It is apparent that the larger the consolidation settlement before shaking, the larger the settlement due to the shaking.

Fig. 19 shows photographs of the embankments of Tests 1-1 and 4-3 after the tests. The area where significant shear deformation occurred coincides with the saturated zone.

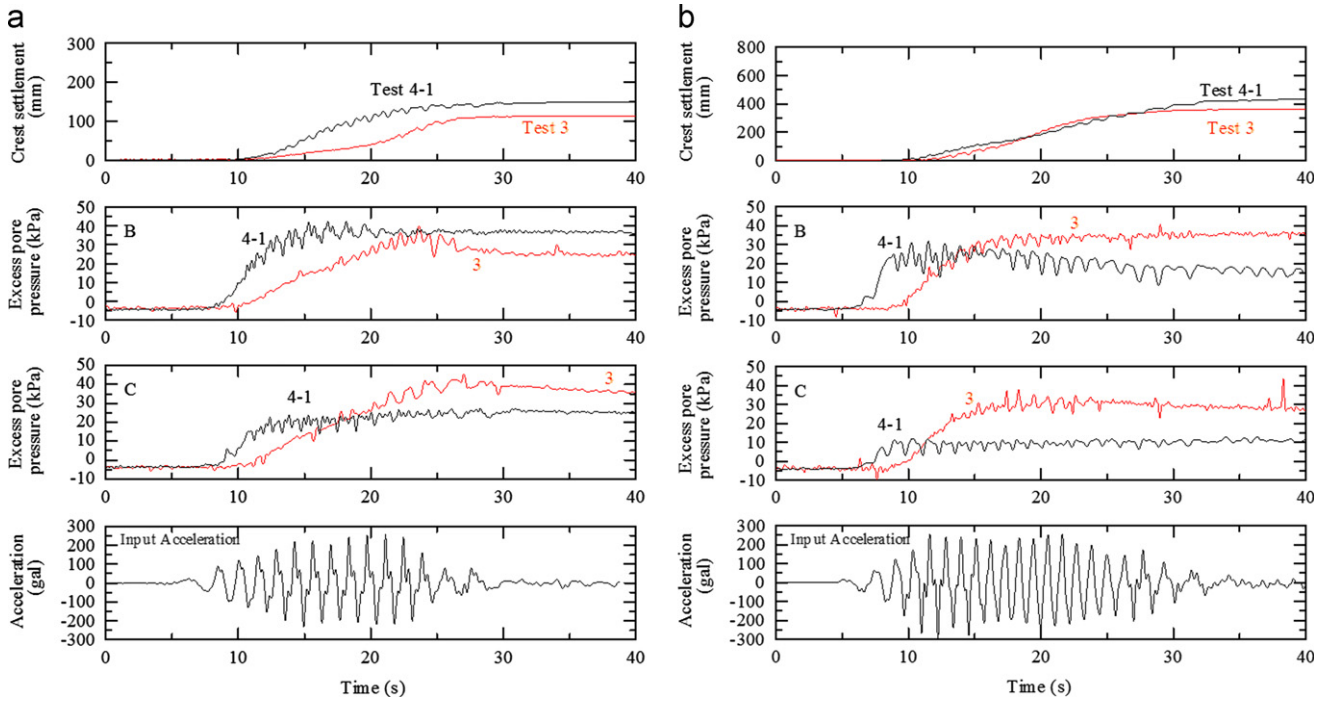

Fig. 16. Selected time histories of excess pore pressures and settlement of Models 3 and 4.

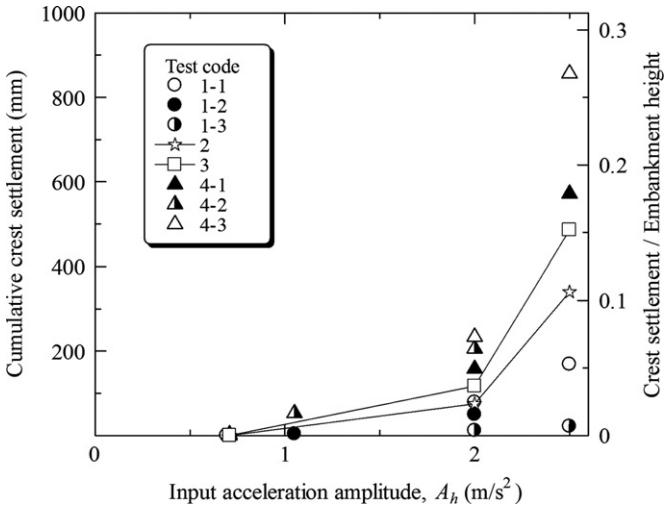

Fig. 17. Effect of consolidation settlement on crest settlement.

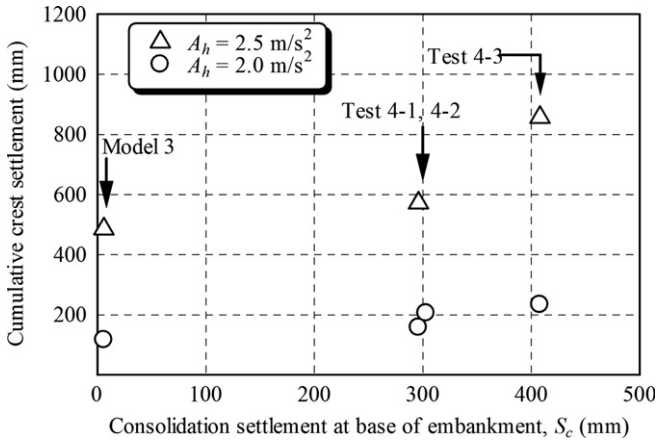

Fig. 18. Summary of crest settlement.

For Test 4-3, the liquefied embankment soil largely spread laterally. The container side wall restricted the soil deformation and the crest settlement might be influenced to some extent for the Model 4 embankments.

In all the tests, large cracks developed from the surface of the crest and the slope to the depth of the saturated zone, which is due to the horizontal tensile deformation of the liquefied zone. Although the crest settlement for Test 1-1 was much smaller than Model 4, the width and the depth of the cracks were as large as those observed in Model 4. As for the field cases reported by Sasaki (2009), Yanagihata et al. (2009), no close correlation between the crest settlement and the significance of the cracks was found and this is the case in this study. It is interesting to note that Tomogane and Okamura (2010) conducted dynamic centrifuge tests on embankments with the same dimensions and properties resting on a liquefiable foundation soil. They reported that no apparent cracks appeared at the surfaces of the embankments, although the embankments subsided as much as 1 m. The groundwater table of their model was 1 m below the surface of the free field and the embankment soil did not liquefy. Similar observations were reported in the literature (Adalier et al., 1998; Okamura and Matsuo, 2002). This fact alludes that the existence of non-liquefiable soil layers underneath embankments helps to maintain embankment integrity even if the embankment undergoes subsidence due to foundation liquefaction.

In this study, simple uniform sand embankments were used to study the influence of the pre-deformation of

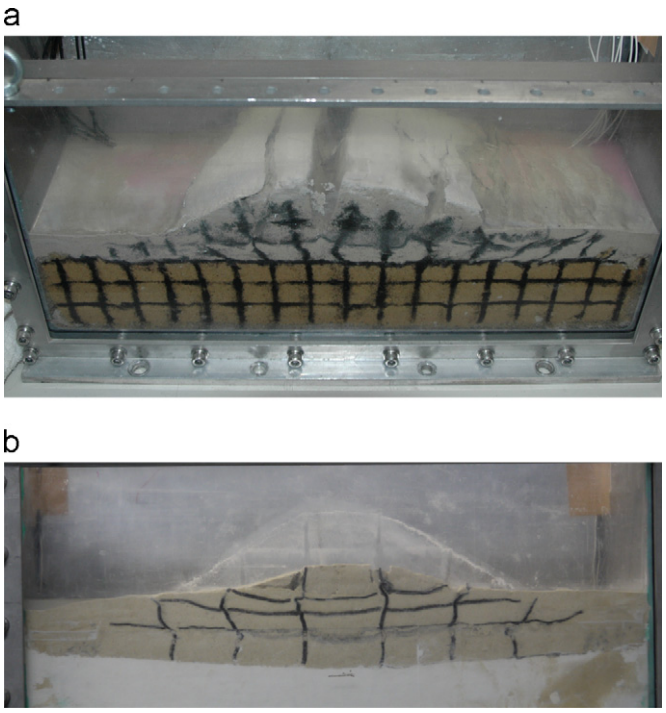

Fig. 19. Photograph of Models 1 and 4 after tests. (a) Test 1-1 (b) Test 4-3.

embankments due to foundation consolidation on seismic stability. On the other hand, the damaged levees have complicated structures composed of different soil zones, as indicated in Fig. 2. The similarity of the deformation observed in this study and that *in situ* is not discussed here. Tests on models which can closely reproduce the *in situ* levee structures will be useful for better understanding the particular embankment failure in this mechanism as well as the validity of centrifuge modeling. Such model tests will be reported elsewhere in the near future.

4. Summary and conclusions

It has been believed that embankments resting on non-liquefiable foundation soils with a level surface are rarely damaged during earthquakes. However, river levees underlain by peat deposits were severely damaged during the 1993 earthquake in Hokkaido and similar case histories have been reported in literature (e.g., Japanese Geotechnical Society, 2010). A reduction in stress in embankments and the degradation of soil density and an increase in thickness of the saturated zone in embankments, all due to the subsidence of the embankments, are surmised as underlying mechanisms. More recently, a large number of river levees was reported to have failed in this mechanism during the 2011 off the Pacific coast of Tohoku earthquake. In this study, centrifuge tests were conducted to look into the effects of deformation and the associated change in stress of embankments caused by compressible foundation soil on the seismic stability of partly saturated embankments.

Regarding the thickness of the saturated zone, higher excess pore pressure and larger crest settlement were observed for cases of thicker zones. The drainage conditions at the embankment base also had a significant influence on the liquefaction behavior of the zone.

For cases of embankments on clay, it was observed that the horizontal stress was apparently lower especially at the lower part of the embankments, if the embankments underwent subsidence due to the consolidation of the foundation clay. For the case of consolidation settlement as high as 13%, the embankment height (Test 4-3), the embankment soil around the bottom center apparently loosened with a volumetric strain of -3%. The rate of generation of excess pore pressure in the saturated zone was higher and the crest settlement was greater for the embankments subjected to large consolidation settlement. This is believed to be due to the combined effect of the stress reduction and the degradation of the soil density, both due to the consolidation settlement.

Cracks with large width and depth were observed for almost all the tests conducted in this study. This is not the case for embankments on liquefied foundation soil. The integrity of an embankment is significantly degraded if the embankment soil liquefies.

Acknowledgements

This research work was partly supported by Grant-in-Aid for Scientific Research (B) Kakenhi No. 21360226 of the Ministry of Education, Culture, Sports, Science and Technology, Japan.

References

Adalier, K., Elgamal, A.W., Martin, G., 1998. Foundation liquefaction countermeasures for earth embankments. Journal of Geotechnical and Geoenvironmental Engineering 24 (6), 500–517.

Garnier, J. 2001. Physical Models in Geotechnics: State of the Art and Recent Advances. First Coulomb Lecture, (CFMS (Eds.)).

Ishihara, K., Iwamoto, S., Yasuda, S., Takatsu, H., 1977. Liquefaction of anisotropically consolidated sand. In: Proceedings of the Ninth International Conference on Soil Mechanics and Foundation Engineering, Tokyo, vol.2. pp. 261–264.

Ishimaru, K., Futagami, O., Okamura, M., Masaoka, T. Inada, S., 2008. Development of mechanical shaker for centrifuge at Ehime University. In: Proceedings of Annual Conference of JGS Shikoku Branch, Takamatsu (in Japanese).

Japanese Geotechnical Society, 2010. Reconnaissance Report of Damage Due to 2010 Maule Earthquake in Chile.

Japan Road Association, 2001. "Specifications for Highway Bridges, Part V, Earthquake Resistant Design." Maruzen (in Japanese).

Koga, Y., Matsuo, O., 1990. Shaking table tests of embankments resting on liquefiable sandy ground. Soils and Foundations 30 (4), 162–174.

Matsuo, O., 1999. Seismic design of river embankments. Tsuchi-to-kiso 47 (6), 9–12 (in Japanese).

Okamura, M., Matsuo, O., 2002. Effects of remedial measures for mitigating embankment settlement due to foundation liquefaction. International Journal of Physical Modelling in Geotechnics 2 (2), 1–12.

Okamura, M., Inoue, T., 2010. Preparation of fully saturated model ground. Proceedings of the Seventh International Conference on Physical Modelling in Geotechnics 2010, in Zurich, vol. 1. pp. 147–152.

Okamura, M., Kiyayama, H., 2008. Preparation of fully saturated model ground in centrifuge and high accuracy measurement of degree of saturation. In: Proceedings of Japanese Society of Civil Engineers 64 (3), 662–671 (in Japanese).

River Front Center, 1999. Personal Communication.

River Bureau, Ministry of Land, Infrastructure and Transport, 2011. 〈http://www6.river.go.jp/riverhp_viewer/entry/y2011eb4071ffc52db6d40a124e92f499b12b83125342f.html〉.

Sasaki, Y., Tamura, K., Yamamoto, M., Ohbayashi, J., 1995. Soil improvement work for river embankment damage by 1993 Kushiro-oki earthquake. In: Proceedings of the First International Conference on Earthquake Geotechnical Engineering, Tokyo, vol. 1. pp. 43–48.

Sasaki, Y., 2009. River dike failures during the 1993 Kushiro-oki earthquake and the 2003 Tokachi-oki earthquake. In: Takaji, Kokusho (Ed.), Earthquake Geotechnical Case Histories for Performance-Based Design. Taylor & Francis Group, London, pp. 131–157.

Shin-etsu Chemical Co., Ltd., 1997. Metolose Brochure, Cellulose Department.

Tohoku Regional Development Bureau, Ministry of Land, Infrastructure and Transport, 2011. 〈http://www.thr.mlit.go.jp/Bumon/B00097/K00360/Taiheiyouokijishinn/kenntoukai/110530/houkokusho.pdf〉.

Tomogane, Y. Okamura, M. (2010). Countermeasures Using Sheet Piles Against Liquefaction-induced Embankment Failure, In: Proceedings of Sixteenth Annual Conference of JSCE Shikoku Branch, Tokushima (in Japanese).

Tan, T.S., Scott, R.F., 1985. Centrifuge scaling considerations for fluid particle systems. Geotechnique 35 (4), 461–470.

Uwabe, T., Kitazawa, S., Higaki, N., 1986. Shaking table tests and circular arc analysis for large models of embankments on saturated sand layers. Soils and Foundations 26 (4), 1–15.

Yanagihata, R., Nakayama, O. Sasaki, Y., 2009. JICE Report 15, pp. 29–32.